Climatic Change (2020) 162:965–988
https://doi.org/10.1007/s10584-020-02772-9

# Late summer temperature variability for the Southern Rocky Mountains (USA) since 1735 CE: applying blue light intensity to low-latitude *Picea engelmannii* Parry ex Engelm

**Karen J. Heeter, et al.** *[full author details at the end of the article]*

Received: 19 June 2019 / Accepted: 16 June 2020 / Published online: 6 July 2020


**Abstract**
Our study examines the application of using blue intensity (BI) methods to develop a late summer maximum temperature ($T_{max}$) reconstruction for the Southern Rocky Mountains—a mid-latitude (i.e., 36° N), arid region in North America. We reconstruct August–September (AS) $T_{max}$ for the period 1735–2015 CE using a composite latewood BI (LWB) Engelmann spruce (*Picea engelmannii* Parry ex Engelm.) chronology from multiple sites across the Sangre de Cristo Mountains in Northern New Mexico, USA. This study presents the first BI-derived temperature reconstruction for the lower mid-latitudes (30–45° N) of North America. We compare the climate response of multiple tree-ring parameters: LWB, earlywood BI (EWB), ΔBI (earlywood BI minus latewood BI), ring width (RW), and maximum latewood density (MXD). Of all parameters, the site-composite LWB and ΔBI chronologies show the strongest correlations with AS $T_{max}$. Reconstructed AS $T_{max}$ demonstrates fluctuating warm and cool periods during the latter portion of the Little Ice Age (ca. 1730–1850) and pronounced warming through the early to mid-twentieth century (ca. 1920–1950s). The reconstruction also documents substantial warming over the last decade, the trend of which appears to be anomalous within the context of the past ca. 280 years. We highlight the potential for BI methods to be successfully used at high-elevation, mid-latitude locations where temperature proxy datasets are scarce or non-existent. As many places across the mid-latitudes lack contiguous, temporally resolved, decadal-scale paleotemperature proxies, we suggest here that BI methods can be effective at improving the spatial gaps in the Northern Hemisphere temperature proxy network.

**Keywords** Blue intensity · North American Southwest · Paleoclimatology · Climate reconstruction · Dendrochronology

**Electronic supplementary material** The online version of this article (https://doi.org/10.1007/s10584-020-02772-9) contains supplementary material, which is available to authorized users.

## 1 Introduction

Climate change is one of the foremost drivers of ecosystem modification (Mooney et al. 2009) and imposes increasing vulnerabilities on both human and natural communities (Thornton et al. 2014). As much of our understanding of climate change relies heavily on the assessment of instrumental data limited to the modern era, proxy datasets are useful tools for better understanding of the effects of human influence on climate variability over longer temporal scales. Warming surface air temperatures over the last century are one of the most widely documented effects of climate change globally (Jones et al. 1999). In North America, increasing annual surface air temperatures are particularly pronounced in the American Southwest and Southern Rocky Mountains region of the USA, where in some areas, average surface air temperatures have increased upwards of 0.6 °C over the last decade (Blunden and Arndt 2016). As this warming trend is expected to continue, mean surface air temperatures are projected to increase across the region by at least 2.5 °C within the next 30 years (Garfin et al. 2014). In 2019, instrumental records documented anomalously warm summer (June–August) mean temperatures across the Southwest United States (US). In August 2016, Utah, Colorado, and New Mexico all experienced the warmest monthly mean temperatures on record (NOAA 2016). The implications of the current warming trend are particularly challenging in the Southwest US, one of the driest regions of the country, where the sustainability of both human and natural systems rely on water resource availability.

The Southwest US has one of the fastest growing regional populations that is projected to increase 68%, reaching to 94 million by 2050 (Jardine et al. 2013). In a region that is expected to only get hotter and drier, projections suggest that increased heat, coupled with changes to warm season (e.g., rainfall) and cool season (e.g., snowpack) precipitations, will drastically affect the lives and economies of over 56 million people.

Recent advances in dendrochronology have allowed for the development of temperature reconstructions of varying spatial scales, ranging from local to hemispheric. Tree-ring-based temperature reconstructions were historically accomplished using instrumental data in combination with chronologies developed from tree-ring parameters such as tree-ring width (RW) or maximum latewood density (MXD). In North America, the majority of tree-ring-derived temperature reconstructions originate from high latitudes (> 50° N), where temperature is expected to be the greatest limiting factor on tree growth (Jacoby and D'Arrigo 1989; Briffa et al. 1992, 2001; Davi et al. 2003; Anchukaitis et al. 2013; Wiles et al. 2014; Wilson et al. 2016). However, the development of MXD and RW networks in the mid-latitudes of the continental US throughout the late 1980s and 1990s (e.g., Briffa et al. 1988, 1992; Schweingruber et al. 1993; Schweingruber and Briffa 1996) increased the density of chronologies which allowed for reconstruction of summer temperatures across portions of the previously under-represented areas of North America. Networks of tree-ring-derived climate proxies, which often also allow for longer-term reconstructions of precipitation and temperature, are necessary to better understand regional spatial patterns of ecosystem response to climate change.

As chronology networks are important for examining current and past climate over large spatial extents, they must be updated regularly to account for the most recent decades and added to in places where the spatial representation of local climate variables by tree-ring parameters is weak or non-existent (Schneider et al. 2015; Stoffel et al. 2015; Wilson et al. 2016). Despite having MXD is a robust parameter for reconstructing past summer temperatures, only a few MXD-derived paleoclimate endeavors have been accomplished within the continental US compared to within Europe, Canada, and the Alaskan US. Compared to ring

width, substantially fewer millennial length MXD records exists for North America (e.g., Luckman and Wilson 2005), especially in the low to mid-latitudes. The high cost associated with producing tree-ring densitometry data is often prohibitive to research institutions. This, in combination with time-consuming laboratory sample preparation requirements, is likely a deterrent to conducting rigorous, widespread updates to existing MXD chronologies so that they account for warming trend since ca. 1990.

In attempts to remedy the issues relating to the time and cost-intensive nature of generating MXD data, the application and skill of alternative tree-ring parameters for temperature reconstructions are increasingly being evaluated. In recent years, refinement of blue intensity (BI) methods have allowed for the development of a temperature-responsive, alternative tree-ring parameter to MXD (McCarroll et al. 2002; Campbell et al. 2007; Björklund et al. 2014; Rydval et al. 2014; Wilson et al. 2014; Linderholm et al. 2015). Early development of BI methods emphasized the use of imaging analysis techniques to examine wood density properties, with the hypothesis that a strongly coupled relationship between reflected visible light in the blue wavelengths and wood density allowed the former to act as a surrogate parameter for the latter (McCarroll et al. 2002). Sheppard et al. (1996) first demonstrated the successful use of reflected light brightness values across earlywood and latewood to reconstruct temperature. As late summer temperatures were found to be influential on the lignification of the secondary cell wall (Gindl et al. 2000) and shorter radiation wavelengths are more readily absorbed by lignin, the strongest association was identified between MXD and brightness resulting from the blue spectrum (McCarroll et al. 2002). Refinement in the analysis of blue spectrum–reflected light and standardization of laboratory methods have resulted in the latewood blue intensity (LWB) parameter producing consistently comparable correlations to temperature as MXD (e.g., Björklund et al. 2015). Further, LWB offers a more time-efficient and cost-effective alternative to MXD for reconstructing temperature (Björklund et al. 2019). Despite these advantages over MXD, most BI studies to date are primarily geographically restricted to the high latitudes. Given that BI methods are relatively new and still in an experimental phase, more studies are needed to evaluate the applicability of BI methods across different regions, especially at high-elevation, low-latitude locations, where certain tree species still produce consistent annual growth rings (e.g., Brookhouse and Graham 2016; Buckley et al. 2018; Heeter et al. 2019). To date, no published BI data exist within the non-Alaskan continental US, and temperature proxy data is especially spatially and temporally limited at high elevations in the mid-latitudes (30–50° N). Further, only a few attempts have been made to reconstruct temperature using tree-ring parameters in the arid Southwest US (Briffa et al. 1992; Schweingruber and Briffa 1996; Salzer and Kipfmueller 2005). If BI methods can be successfully used to reconstruct summer temperatures in places where MXD records are either absent or temporally limited, this technique may improve the incomplete spatial and temporal coverage of paleoclimate records across North America and elsewhere. We identified the Southern Rocky Mountains region of the USA (southern Colorado, Northern New Mexico) as a prime area to evaluate novel methods of developing tree-ring-based climate reconstruction for a variety of logistical and environmental reasons. The Southern Rocky Mountains has adequate spatial and continuous temporal coverage of instrumental station data capable of documenting temperature trends since the turn of the twentieth century. Additionally, the complex relief of the Southwest US allows for local dominance and persistence of many long-lived, temperature-limited tree species growing at high elevation (> 3000 m). Similar to how they perform at high latitudes, temperature proxies have historically been most successful at high altitudes, where inter-annual climate variability strongly influences tree growth as the

limiting factor (Fritts 1976). Because of its persistence at high elevations and latitudes, Engelmann spruce (*Picea engelmannii* Parry ex Engelm.) has been shown to be an exceptional species for developing climate reconstructions from tree-ring data (Parker and Henoch 1971; Wilson and Luckman 2003). This long-lived (> 600 years), shade-tolerant, canopy-dominant species occupies a range extending from British Columbia in the north, through the Western US and becomes disjunct at the southern range extent in south-central New Mexico (NM). At its southern range periphery, Engelmann spruce becomes less dominant, as its distribution becomes scarcer and is limited to near tree line (Alexander and Sheppard 1984). Engelmann spruce habitat is typically characterized as humid with long, cold winters and short, cool summers, with heavy snowfall and extreme temperature ranges. This habitat is considered one of the highest-elevation and coldest forest environments in the non-Alaskan continental US.

In this study, we assess the efficacy of using BI methods within the mid-latitudes of the Southern Rocky Mountains using three Engelmann spruce sites distributed across Northern NM. Our successful demonstration of the ability of the LWB metric to track late summer maximum temperature ($T_{max}$) enabled us to develop a temperature reconstruction for the northern Sangre de Cristo range of north-central NM. We reconstructed late summer (August–September) $T_{max}$ using a composite Engelmann spruce LWB chronology spanning the period 1735–2015. Further, we enhanced our assessment of the application of BI methods with the examination of pre-existing RW and MXD data available within our immediate study area. Our study highlights the potential of using BI methods to produce larger-area temperature reconstructions for the mid-latitudes encompassing the American Southwest and elsewhere across the Western US.

## 2 Methods

### 2.1 Study area

Our study area comprises three Engelmann spruce sites located at the southern geographical range limit of the species within the Sangre de Cristo Mountains, Northern NM: Wheeler Peak (WHE) (36.57° N, − 105.42° W), Serpent Lake (JIS, near Jicarita Peak) (36.06° N, − 105.56° W), and San Leonardo Lakes (SLE) (36.00° N, − 105.65° W) (Little and Viereck 1971; Fig. 1). The sampling elevation at the WHE and JIS sites was between 3400 and 3600 m, which was at or near tree line at these sites (Fig. 1, Table 1). At SLE, however, steep (> 40°), unstable talus slopes restricted us to sampling at 3450 m, despite tree line being located at ca. 3750 m. Instrumental data obtained nearest to our sample locations indicate the local climate is characterized by minimum monthly average temperatures ranging from − 11.8 in January to 11.1 in July, and maximum monthly average temperatures ranging from 4.2 in January to 29.2 in July. Annual precipitation ranges from 13.9 mm in February to 52.3 mm in August (averaged 1895–2018; US Climate Data 2019). For our study region, July and August are characterized as having the highest average maximum temperatures (29.2 and 27.7, respectively) as well as receiving the greatest amount of monthly precipitation (36 mm and 48 mm, respectively) (US Climate Data 2019).

### 2.2 Sample collection

At each site, we collected increment cores from the largest-diameter and oldest-looking Engelmann spruce individuals between 3500- and 4000-m elevations. All cores were extracted

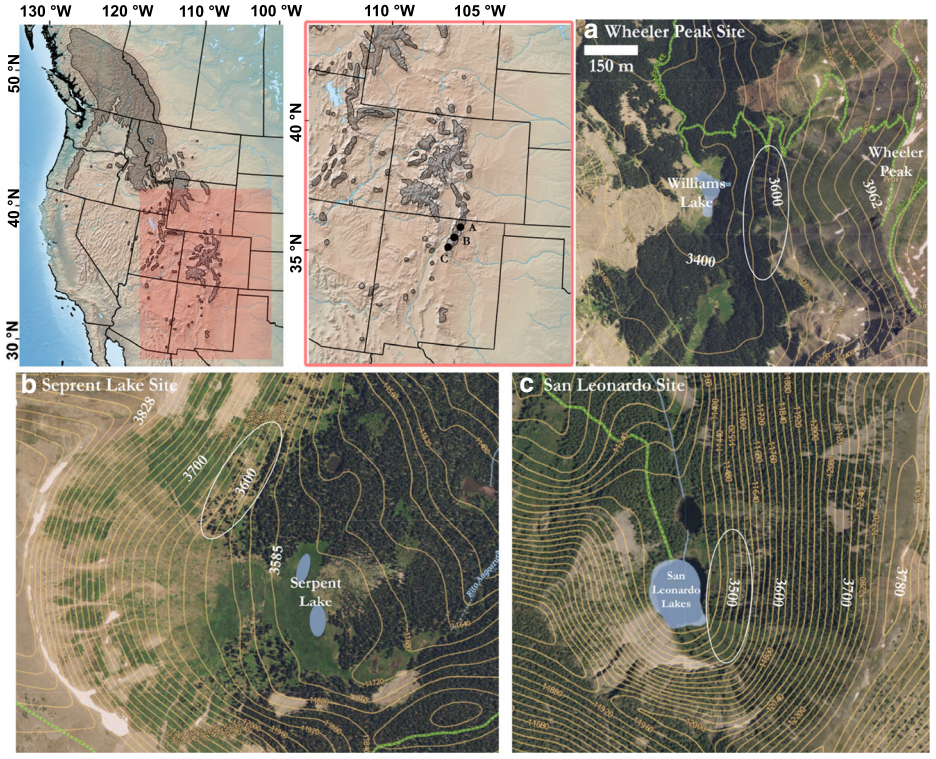


**Fig. 1** Map showing the locations and topographic settings (contours) of the three Engelmann spruce sites sampled for blue intensity, including **a** Wheeler Peak (WHE), **b** Serpent Lake (JIS), and **c** San Leonardo Lakes (SLE) sites within the Sangre de Cristo Mountains, NM, located at the southern range limit for the species (gray polygon; Little and Viereck 1971). Approximate tree sampling locations and elevations at each site are circled. Green lines in panels **a**–**c** represent hiking trails

**Table 1** Site location and chronology

| | WHE | JIS | SLE |
|---|---|---|---|
| Latitude (° N) | 36.65 | 36.06 | 36.00 |
| Longitude (° W) | 105.42 | 105.56 | 105.65 |
| Sampling elevation (m) | 3600 | 3600 | 3450 |
| RW | | | |
| No. of cores (trees) | 26 (16) | 27 (20) | 18 (13) |
| Full period | 1667–2015 | 1637–2014 | 1653–2015 |
| BI | | | |
| No. of cores (trees) | 26 (16) | 27 (20) | 18 (13) |
| Full period | 1667–2015 | 1637–2014 | 1653–2015 |
| MXD | | | |
| Elevation | 3120 | – | – |
| No. of cores (trees) | 20 (10) | – | – |
| Full period | 1830–1983 | – | – |

Ring width, blue intensity, and maximum latewood density information for the Wheeler Peak, Serpent Lake, and San Leonardo Lakes study sites within the Sangre de Cristo Mountains, Northern NM

*WHE* Wheeler Peak, *JIS* Serpent Lake, *SLE* San Leonardo Lakes, *RW* ring width, *BI* blue intensity, *MXD* maximum latewood density

[a] Information from Briffa et al. (1992)

at breast height (1.3 m above ground surface) using a 5.0-mm diameter increment borer. We sampled two cores from each tree parallel to the contour of the slope to reduce abnormalities in ring growth (Stokes and Smiley 1968). We targeted trees that showed minimal outward evidence of landslide, insect, or wind damage. We collected a total of 32 increment cores from 16 trees at WHE, 54 cores from 27 trees at JIS, and 44 cores from 22 trees at SLE.

### 2.3 MXD data compilation

We gathered the MXD raw measurement dataset for WHE from the International Tree-Ring Data Bank (ITRDB) (Briffa et al. 1992). The MXD dataset from WHE spans the period 1830–1983, and increment cores were collected from trees at 3120 m.

### 2.4 Chronology development

While the development of BI methods is still in relative infancy compared to MXD, and due to the fact that BI-derived data produced by different laboratories are likely to be combined across regions, the importance of ensuring methods is standardized within the context of accuracy and precision is paramount (Björklund et al. 2019). Engelmann spruce cores were dried and mounted, then sanded at 220, 400, 600, and 1000 American National Standards Institute (ANSI) grit increments. Cores were finished by hand sanding with a 9-μm film (Speer 2010). Because the Engelmann spruce wood collected at these sites is characterized by a light color and generally does not exhibit any discoloration due to heartwood/sapwood differences or resins, no chemical pigment extraction, often necessary for BI methodology, was required for our samples. Before scanning, all samples were first cross-dated visually using a × 40 microscope.

We first calibrated our scanner to ensure accuracy of generated BI values, then scanned all samples at 2400 dpi on an Epson Expression 12000XL scanner using an IT8.7/2 calibration card coupled with the 89 SilverFast software to ensure replication. We scanned a total of 52 series. We conservatively excluded cores from scanning if they possessed excessive amounts of traumatic resin ducts that formed across the entire radial width of an annual ring, because a failure to avoid these cellular abnormalities results in inaccurate blue reflectance values. We also excluded cores that had continuous blue fungal stain. Although initial field sample collection was specifically designed to target the oldest trees with no outward obvious signs of insect, landslide, or wind damage, all agents which increase the likelihood of these types of wood abnormalities, we still removed between two and four cores from each site dataset for this reason. After cores were scanned, we delineated growth ring boundaries using automated detection in the program CooRecorder (Larsson 2014) to generate RW values to the nearest 0.001 mm precision.

After obtaining RW measurements, we checked our dating accuracy using the software COFECHA (Holmes 1983). Once we were confident that all samples were accurately dated, we collected BI values using the CooRecorder software wood BI (LWB) and ΔBI data. Although Engelmann spruce collected from our sites did not show any sapwood/heartwood color changes, we decided to collect and examine the ΔBI metric to further explore the climate response and relationship between ΔBI and LWB. Because samples exhibited moderate age-related trends, we detrended the Engelmann spruce RW, MXD, LWB, and ΔBI series. Since raw LWB is negatively correlated with MXD, we inverted the raw LWB data to allow for detrending of the data by methods similar to those used for MXD data (Rydval et al. 2014). We

initially used interactive detrending to examine the effects of various conservative smoothing splines within the signal-free detrending (SFD) (Melvin and Briffa 2008) framework (Figure S1). All series were standardized using the power-transformed residuals. We detrended the ΔBI data similarly to the LWB data, because the calculation of this metric inherently results in a positive correlation between inverted LWB and ΔBI (Wilson et al. 2017a). We ultimately detrended the RW, BI, and MXD data using the age-dependent spline (ADS) (Melvin et al. 2007) within the SFD framework, because the ADS produced the best curve fit to the data. This combination also best reduced the medium-frequency distortion (e.g., over-exaggeration) at the beginning and end segments of our chronologies (e.g., the twenty-first-century climate warming trend) resulting from the curve fitting process. Similar to this study, Wilson et al. (2019) also apply this detrending approach to both RW and LWB for the purpose of examining relationships between growth/density and summer temperatures. We used the expressed population signal (EPS; Wigley et al. 1984) with an arbitrary threshold of 0.80 to help evaluate the quality of our chronologies and to determine the period over which we had sample replication adequate for developing a reconstruction.

### 2.5 Climate response

We used the Pearson correlation analysis to test temporal relationships between temperature data and RW, MXD, earlywood BI (EWB), LWB, and ΔBI data using the treeclim package in R (Zang and Biondi 2015). Further, we used the KNMI Climate Explorer (Trouet and Van Oldenborgh 2013) to assess spatial correlations between temperature data and RWI, MXD, EWB, LWB, and ΔBI data. We performed these tests using monthly $T_{max}$ and mean temperature ($T_{mean}$) from the parameter-elevation relationships on independent slopes model (PRISM) (Daly et al. 1994) surface temperature dataset at 4k resolution and averaged over the Southern Rocky Mountains (37.25–35.90° N, 104.15–106.05° W). Prior examination of all tree-ring metrics (RW, MXD, and BI metrics) with minimum temperature indicated either no or very weak significant relationships; thus, we excluded minimum temperature as a variable in any subsequent analysis for this study. We chose to use PRISM data because this gridded data product adequately provides high-spatial resolution monthly temperature data that performs well in regions characterized by complex terrain, such as in the heavily dissected landscapes of the Southern Rocky Mountains. While PRISM pulled temperature data from multiple stations in the region (Table S1), the primary data source for the area encompassing our sample area is Red River, a rural station located in cool conifer mountain terrain at 2644 m and provides temporally reliable and consistent temperature data from 1906 to 2015. Correlations were calculated over the period 1895–2015. We tested for signal stability by performing forward moving interval correlation analysis using treeclim (Zang and Biondi 2015). We assessed the spatial homogeneity between the three site chronology signals using principal component analysis (PCA) across all series over the well-replicated common period (1735–2015). Further, we examined the spatial loadings of the individual chronologies based upon the most prominent principal component (e.g., Wilson et al. 2007b).

### 2.6 Climate reconstruction

We chose a principal component regression (PCR) technique to reconstruct late summer maximum temperatures (August–September (AS) $T_{max}$) for the Southern Rocky Mountains. We initially pre-whitened the BI data and temperature data to provide a conservative estimate

of BI-climate relationships that did not exhibit inflation due to auto-correlation. We used three correlation tests—Pearson, robust Pearson, and Spearman—to examine the BI-climate relationships and retained chronologies that were significantly ($p < 0.01$) related to AS $T_{max}$ over the common period (1907–2015). For BI series which were significant, their original, non-prewhitened chronologies were included in the PCR. Following the Kaiser-Guttman rule (Guttman 1954; Kaiser 1960), we retained the first $n$ eigenvectors with eigenvalues > 1.0 for the multiple regression. We determined the final subset of PCs by using the minimum Akaike information criterion (AIC), which includes a penalty term for increasing the number of predictors in the model (Akaike 1974).

We split the instrumental period (1907–2015) into two equal periods termed the early period (1907–1961) and late period (1962–2015) to validate and cross-validate the AS $T_{max}$ reconstruction model (Table S5). To ensure stability over time, model validation was performed by calculating calibration statistics for the early period (1907–1961) and verification statistics for the late period (1962–2015), and vice versa. We used two goodness-of-fit tests to validate the models: the reduction of error (RE) and coefficient of efficiency (CE) statistics (Fritts 1976; Cook et al. 1999). When RE values (ranges from $-\infty$ to + 1) are positive, the calibration model is a more skillful predictor of the target data than the mean of the instrumental data during the calibration period. Although CE has the same range and calculation, a positive CE value is more difficult to obtain because it relies on the verification period mean for a baseline of predictive skill. The validation statistics produced were calibration and verification period coefficient of determination ($CR^2$ and $VR^2$), validation period reduction of error (VRE), validation period coefficient of efficiency (VCE), and root-mean-square error (RMSE). After successful determination that the model is time-stable, we used linear regression to estimate AS $T_{max}$ calibrated over the full PRISM 4k instrumental period (1907–2015) with the composite LWB chronology, and evaluated the model residuals for linear trends and first-order auto-correlation (Durbin-Watson statistic) (Durbin and Watson 1971).

To assess model uncertainty, we used the maximum entropy bootstrapping (MEBoot) method (Vinod and López-de Lacalle 2009) to produce 1000 reconstruction replicates. We used the MEBoot method because it produces an empirical probability distribution for each reconstructed estimate (e.g., each year) on which the estimation of uncertainty is based (Cook and Kairiukstis 2013). Additionally, the MEBoot method does not assume stationarity and preserves the auto-correlation structure of the time series, and calculations of uncertainty estimates for the calibration and verification statistics are semi-parametric (Cook et al. 2013).

## 3 Results and discussion

### 3.1 Signal strength and homogeneity

Individually, WHE contains 26 series, spanning the period 1667–2015 for RW, EWB, LWB, and ΔBI data (Table 1). MXD data for WHE contains 20 series and spans the period 1830–1983. JIS is comprised of 27 series and spans the period 1637–2014. SLE contains 18 series and spans the period 1653–2015. For the period 1637–2014, SLE contains 18 series and spans the period 1653–2015. For each individual site, both mean inter-series correlation (RBar) and EPS values indicate that RW maintains the strongest common signal over the period where the EPS is > 0.80 in comparison with BI and MXD (Table 2). The RBar for RW across the three

sample sites is 0.57 (ranging 0.54–0.59). For EWB, the RBar is 0.27 (ranging 0.26–0.27). For LWB, the RBar is 0.28 (ranging 0.25–0.31), which is comparable with the EWB RBar and the ΔBI RBar of 0.31 (ranging 0.29–0.35). The RBar for MXD, which comprised of only one site (WHE), is 0.49.

The mean number of series from across the three sites required to meet an arbitrary EPS value of 0.80 is 3 for RW, 10 for EWB, 11 for LWB, 9 for ΔBI, and 5 for MXD. At each site, BI requires at least three times the amount of measured series than RW to meet the EPS threshold. This is consistent with other BI studies conducted in North America and Europe, which suggests that one of the caveats of BI is that it requires substantially more trees to reach the point of theoretical infinite replication and maintain a signal adequate for developing a reconstruction (Wilson et al. 2017a, 2019). The development of local networks comprised of data obtained across multiple nearby sites, such as in the case we present here, can be an effective way to overcome this problem of low sample depth. The LWB signal in the Southern Rocky Mountains is surprisingly strong for the relatively few trees needed to reach the EPS threshold (Table 2). This may be attributed to increased commonality in growth response among individuals across these three study sites, or potentially be a result of increased densiometric (here, referring to the process of latewood lignification) synchrony of Engelmann spruce compared to other species (e.g., *Picea glauca*, white spruce). Similarly, the RBar values for RW at each site are almost twice as high as those for BI. However, MXD displays superior signal commonality to BI, second to RW. Comparatively, MXD, like RW, requires fewer samples to achieve a strong common signal. The RBar is also more comparable to RW than to any BI metric. Both EWB and the LWB have comparable signal commonality to ΔBI. This similarity can be expected due to the nature of the calculation of ΔBI, as ΔBI quantifies the difference between BI measurements collected from the earlywood and latewood zones of the annual ring.

Overall, tree-ring metrics across each site correlate strongly with one another (Table S2). Strong, positive correlations ($p < 0.01$) between metrics across different sites suggest a strong spatial correspondence between overall growth and physiological response of same-species individuals at closely situated sample sites. The high level of agreement between tree-ring

**Table 2** RBar and the number of series needed to attain an EPS of 0.80 for all individual sample sites (Wheeler Peak (WHE), Serpent Lake (JIS), and San Leonardo Lakes (SLE))

| | WHE | JIS | SLE | Mean |
|---|---|---|---|---|
| RW RBar | 0.590 | 0.586 | 0.540 | 0.572 |
| No. series EPS | 3 | 3 | 4 | 3 |
| Year EPS 0.80 | 1699 | 1709 | 1707 | 1705 |
| EWB RBar | 0.259 | 0.262 | 0.274 | 0.265 |
| No. series EPS | 9 | 10 | 12 | 10 |
| Year EPS 0.80 | 1800 | 1759 | 1778 | 1779 |
| LWB RBar | 0.309 | 0.286 | 0.252 | 0.282 |
| No. series EPS 0.80 | 9 | 11 | 12 | 11 |
| Year EPS 0.8 | 1797 | 1768 | 1802 | 1789 |
| ΔBI RBar | 0.294 | 0.350 | 0.295 | 0.313 |
| No. series EPS 0.8 | 10 | 8 | 10 | 9 |
| Year EPS 0.80 | 1804 | 1737 | 1818 | 1786 |
| MXD RBar | 0.493 | – | – | – |
| No. series EPS 0.80 | 5 | – | – | – |
| Year EPS 0.80 | 1833 | – | – | – |

For RBar values, all data were detrended using the age-dependent spline in the signal-free framework (AD-sf)

metrics at these three sites was the motivation to develop a composite chronology. As LWB, like MXD, acts as a representation of latewood density (Björklund et al. 2019), we should expect similar trends of cross-metric correlations between BI and RW as between MXD and RW. Under this assumption, we should expect that MXD is more highly correlated with LWB than with RW. As raw LWB data displays an inverse relationship with MXD, high correlations found between MXD and the inverted LWB is consistent with the literature. Surprisingly, the MXD taken from WHE correlates higher with JIS ΔBI ($r = 0.57$) than WHE LWB or WHE ΔBI ($r = 0.48$ and 0.34, respectively). This is likely a result of differences in sampling locations of WHE MXD and WHE BI/RW, as WHE MXD was collected at a significantly lower elevation (Table 1) and from different trees than those for WHE RW/BI. Across the three sites, SLE and JIS have the weakest positive correlation for the LWB variable. For each individual site, EWB has the weakest coupling with RW of all BI metrics, followed by LWB and ΔBI (Table S2).

While the BI chronologies display strong signal commonality for the most recent 200 years, they are not adequately replicated enough to meet an EPS value of 0.80 prior to 1786. The separate PCAs for RW, EWB, LWB, and ΔBI over the period 1735–2015 revealed similar loadings for each of the four variables. The explained variance on the first eigenvector is 40.9% for RW, 30.7% for EWB, 35.3% for LWB, and 30.8% for ΔBI (Table S3). In comparison to a series originating from WHE and SLE, a series from JIS load weakly to PC1. This difference in loading is likely partially influenced by varying microtopographical variables and JIS being the only site located on an east aspect rather than a west aspect. Based on PCA results, a series from individual sites were pooled into one regional composite chronology for RW, EWB, LWB, and ΔBI to maximize signal commonality over a longer time period. Our resulting composite chronologies for each parameter are better replicated over longer periods of time compared to individual site chronologies. Additionally, these composite chronologies allow for direct comparisons of multiple tree-ring parameters and for the better examination of various detrending techniques. While the composite chronologies extend from 1635 to 2015, chronology variants for RW, EWB, LWB, ΔBI, and MXD (Figure S1) indicate that these composite chronologies have adequate signal commonality and sample representation (EPS > 0.80) back to 1735. The composite RW chronology displays the highest amount of common signal variability (RBar = 0.33) and maintains an EPS > 0.80 to 1713 (Table S4). The LWB composite chronology shows the second highest common signal (RBar = 0.29) and maintains an EPS > 0.80 to 1738.

The examination of using various detrending methods resulted in relatively similar resultant chronologies, especially in most recent 100 years, for all tree-ring metrics except for the EWB parameter. The LWB chronology shows the least sensitivity to various modes of detrending compared to all other tree-ring metrics examined in this study (Figure S1). The two-third and NEGEXP smoothing splines over- and under-exaggerate, respectively, the end effects of the EWB chronology post 1950. All modes of detrending show the greatest amount of variability prior to 1800, where the sample depth is comparatively lower. For RW, EWB, LWB, and ΔBI, the chronology versions using the two-third spline track the ADS variants, the most similarity. From 1653 to present, the NEGEXP variants for composite RW, LWB, and ΔBI chronologies display lower mean $z$ scores over this period and thus show higher variance from 1653 to 1800 (period where EPS < 0.80) than the two-third spline and ADS variants. This exaggerated decrease in early period mean chronology values exemplifies the *end effect* artifact from applying a stiff, linear curve fit model to the data. We ultimately used a constrained ADS to minimize the loss in climate signal in the most recent period (Wilson et al. 2019). Compared to

the composite RW chronology, the composite chronologies for all BI metrics show less variability over the entire period. This is consistent with other similar studies, which compare variants of RW and LWB (e.g., Wilson et al. 2019). The lower-frequency (e.g., multi-decadal to centennial) signals are greatly affected by both the mode and practice of detrending (Figure S1), as well as by innate proxy characteristics (e.g., changes in series length and sample depth). This notion is the impetus for further examination into the effects of combinations of such variables for continual refinement of novel methods in developing paleoclimate proxy records from natural sources (e.g., BI from tree rings). The EPS value intermittently waivers around 0.80 for LWB and ΔBI between 1725 and 1760 before consistently dropping below the 0.80 threshold. From here, we limit further analysis of our composite tree-ring chronologies to the period 1735–2015, where we have adequate sample replication across all tree-ring metrics.

### 3.2 Climate response and regional expression

Our climate response analysis of RW, EWB, LWB, and ΔBI is conducted over the period 1907–2015, where there is continuous data from at least two individual stations within the sample region. Within the Sangre de Cristo Mountains range of the Southern Rocky Mountains (37.25–35.90° N, 104.15–106.05° W), all parameters are more strongly correlated with $T_{max}$ than $T_{mean}$ (Table S4). At each individual site, AS $T_{max}$ consistently shows the strongest relationships with both BI metrics (Fig. 2a). The pooling of series from all sites into one regional chronology improves the climate response of all three BI metrics to AS $T_{max}$ (Fig. 2a). Individually, RW shows a minor positive response to AS $T_{max}$ at JIS and SLE but does not exhibit any significant response when pooled into the composite chronology. The lack of temperature signal of RW found here differs from signals found from RW in spruce-dominated boreal forests of higher latitude studies (e.g., Wilson et al. 2019; Luckman and Wilson 2005). We suggest that RW shows less of a temperature response because even though these high-elevation spruce-dominated forests of Northern NM are more humid than most other areas of the Southwest US, the comparatively arid climate still heavily influences patterns of radial growth. We examined this further by running correlation tests for all composite chronologies against PRISM 4k precipitation data from the same spatial and temporal extents used to examine PRISM temperature data (Table S5). Although RW is the only metric that shows a weak, positive correlation with precipitation (current and previous year (− 1) data) over the entire 1907–2015 period, this metric does show strong, positive correlations with May (− 1) precipitation over the period 1980–2015 ($r = 0.54$, $p < 0.01$). This increasing response of RW to precipitation is coupled with decreased sensitivity to temperature in the most recent period (Figure S4) and suggests the possibility of precipitation becoming an increasingly limiting factor on radial growth at high elevations within this region. EWB, LWB, and ΔBI show significant negative correlations with current year August precipitation. Similar to the trend seen with RW, these relationships strengthen after 1980. Here, the data suggest that changes in precipitation are increasingly influenced by changes in temperature (e.g., twenty-first century warming). This modern trend is well documented across other parts of the Southwest US (Weiss et al. 2009; Cayan et al. 2010; Harley et al. 2020).

The strongest relationship with temperature exists between LWB and seasonal $T_{max}$ ($r = 0.64$). The regional LWB chronology is also a strong predictor of $T_{mean}$ ($r = 0.54$). The temperature signal of the EWB composite chronology is weaker and more spatially limited than the signals found in the LWB and ΔBI composite chronologies. Examination of EWB

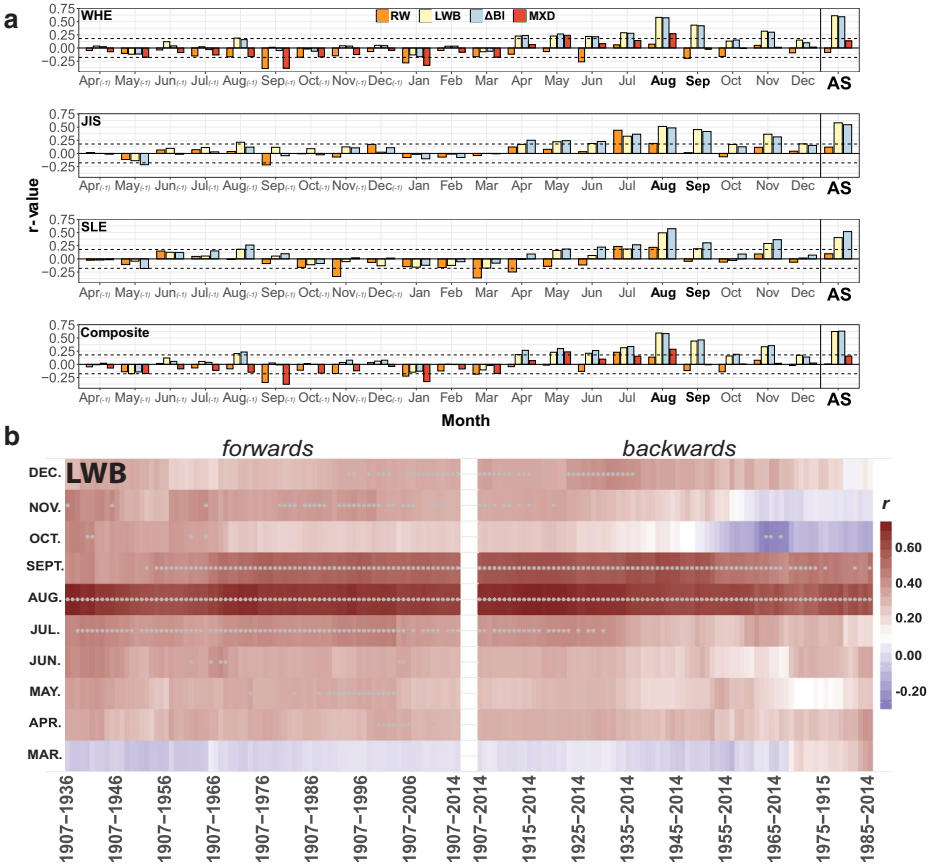


**Fig. 2** **a** Monthly climate response of tree-ring metrics (RW, LWB, ΔBI, and MXD) to regional PRISM 4k $T_{max}$ data for both the individual sites (WHE, JIS, SLE) and the AD-sf-detrended composite chronologies from previous year April (Apr (− 1)) through current year December. Climate response is calculated from previous year April (Apr (−1 )) to current year December over the period (1907–1983), and dashed line represents $\alpha$ = 0.05. **b** Forward and backward (evolutionary) moving correlations (gray dots represent $\alpha$ = 0.05) of composite. LWB chronology and regional PRISM 4k AS $T_{max}$ over the period 1907–2015

from these sites indicates that while the composite chronology shows significant positive relationships with both AS $T_{mean}$ and AS $T_{max}$ over the entire tested observational period ($r$ = 0.21 and 0.37, respectively), the temperature signal strength is spatially limited beyond the extent of the immediate study area (Figure S3). Additionally, the EWB metric shows significant positive correlations with March $T_{max}$ in the more recent decades (1960–present) (Figure S4). This trend warrants further examination, as it may have important implications regarding the recent phenomenon of the earlier onset of spring warming in the region, especially within the context of examining differences in the anatomical basis for density between earlywood and latewood (e.g., Björklund et al. 2017). Changes to the seasonal timing and pace of spring snowmelt driven by rapidly warming spring temperatures in the latter twentieth century are well documented across the Western US (Cayan et al. 2001; Westerling et al. 2006); Cayan parameter has not yet been widely examined (e.g., Björklund et al. 2014, 2017; Buckley et al. 2018), and future studies examining the temperature sensitivity of the EWB parameter warrant additional consideration.

To compare climate response of the WHE MXD data to the other metrics, we conducted additional analysis over a shortened period (Table S4), which only includes the years during which MXD is represented (1907–1983). Compared to LWB, the climate response of MXD to AS $T_{mean}$ and $T_{max}$ is relatively low. This is consistent with results using these same MXD chronology data by Briffa et al. (2002). Strictly comparing LWB and MXD at WHE, there is a slight seasonal response difference between these two metrics. The decoupling of late-growing season temperature response between MXD and LWB is somewhat inconsistent with findings from other studies comparing climate response of MXD versus BI at higher latitudes (e.g., Björklund et al. 2014, 2015; Wilson et al. 2014; Fuentes et al. 2018; Kaczka et al. 2018). Instead, at WHE, MXD appears to have improved temperature response throughout the majority of the growing season (May–August) (Figure S4). The difference in monthly climate response between LWB and MXD may be influenced by the ways in which each individual proxy represents lignification, as this process occurs after all radial cell growth has ceased at the end of the growing season (Gindl et al. 2000). While slight seasonal differences between the temperature response of MXD and LWB at WHE are likely due to the innate proxy characteristics themselves, we also consider the influence of differing sample locations for each proxy (e.g., differences in individual trees sampled, topographic position of sampled trees). For example, while both MXD and BI data originate from samples collected at WHE, MXD samples were taken from trees located at a lower elevation and different aspects. We suggest that future studies aiming to develop paleotemperature proxies from BI methods in the Southwest US should consider sampling at high elevation as possible in order to capture the most robust temperature response from samples. Moreso, additional exploration is needed to better understand the influence of microtopography on temperature-limited trees in the mid-latitudes of North America (e.g., Büntgen et al. 2008).

We assess the temporal stability of positive relationships between PRISM 4k AS $T_{max}$ data from the study region and RW, EWB, LWB, and ΔBI over the period 1907–2015, as well as the stability for MXD over the period 1907–1983 (Fig. 2b, Figure S4). Both the forward and backward moving correlation analyses indicate that the relationships between AS $T_{max}$ and LWB and ΔBI are strong over the entire instrumental period. However, LWB shows less weakening in the relationship with temperature than ΔBI. We suspect the weakening in the ΔBI signal is likely attributed to the influence of the EWB data used for the calculation of the ΔBI data. MXD shows temporal stability similar to that of ΔBI, but only for the month of August. RW generally shows a weak and temporally unstable relationship to $T_{max}$ over the test period. However, RW does show a significant ($p < 0.01$) negative relationship with March $T_{max}$ in the most recent decades. RW also shows weak but significant positive correlations with August $T_{max}$ in the early instrumental period (1910–1960) but exhibits a high degree of divergence from instrumental temperature data after 1960. We suspect that the weak and unstable RW-temperature signal is partially due to the presence of the strong previous spring precipitation signal in the composite RW chronology (Table S5). These data suggest that warmer-than-average spring temperatures could have an increasingly negative affect on overall radial growth of Engelmann spruce at high elevations in this region, and that ring width is not an adequate parameter for capturing and preserving a temperature signal. Further, the data support that within this region of the Southern Rocky Mountains, precipitation is becoming more of a limiting factor on radial tree growth than in previous decades.

The time stability of the composite LWB chronology over the full instrumental period is notable for this region. Unlike many of the extant RW-based chronologies encompassing the Western US—including the composite RW chronology presented in this study—the composite

LWB chronology does not exhibit a high degree of divergence (Wilson et al. 2007a; D'Arrigo et al. 2008) from regional temperature data in the most recent decades. As this is the first known publication of a LWB chronology published for this region, this study demonstrates the potential for this tree-ring parameter to improve the spatial resolution of temperature proxy records that adequately capture climatic trends of the most recent decades over broader regions (e.g., gridded network reconstructions). For example, hemispheric-scale temperature reconstructions, such as the temperature reconstruction for the Northern Hemisphere presented by Wilson et al. (2007a), used two chronologies from the mid-latitude continental US (Biondi et al. 1999; Salzer and Kipfmueller 2005) due to the limited number of adequately temperature-responsive tree-ring chronologies in this area. While using a small number of tree-ring chronologies to accomplish a broad-scale, gridded network of temperature reconstructions may not be overly problematic due to the highly auto-correlated nature of instrumental temperature data, increasing the density of robust tree-ring-based temperature proxy datasets will likely lead to subregional improvements in predictive skill for such reconstruction efforts. As the development and integration of BI methods at lower-latitude, temperature-limited locations continues to enhance the field of dendroclimatology, we suspect that the modern period can be adequately captured with the use of BI methods, in conjunction with MXD, to improve understandings of the temporal and spatial variability of past temperatures.

Compared to other tree-ring metrics explored in this study, LWB shows the strongest and most spatially resolved temperature signal over the entire instrumental period (Figure S3). As expected due to the nature of the calculation, the strength and spatial distribution of correlations between ΔBI and AS $T_{max}$ most resembles that produced by the LWB chronology. However, because we see no necessity to use the ΔBI metric due to heartwood/sapwood color homogeneity in our composite chronology series, we limit further examination of BI methods for late summer temperature reconstruction to the LWB metric. The spatial distributions of correlations produced by both the non-transformed and first-differenced versions of the composite AD-sf LWB chronology and PRISM 4k $T_{max}$ closely resemble one another (Figure S2). Both non-transformed and first-differenced versions of the LWB chronology demonstrate strongly ($r > 0.50$) significant ($p < 0.01$) relationships between the study area surface air temperatures and the temperatures over the greater geographic area extending north-south along the Southern Rocky Mountains region (39.0–37.0° N, 106.0–105.0° W) of New Mexico and Colorado. While the non-transformed version of the LWB chronology shows the strongest ($r > 0.60$) relationship with maximum temperature within the immediate study area, with the centroid of the strongest spatial correlation located along the Sangre de Cristo range, the first-differenced chronology indicates a northward shift of the highest spatial correlations centered around the Rio Grande National Forest in southern Colorado. Additionally, the first-differenced chronology shows greater spatial smoothing and more concentric diffusion of the regional expression. Overall similarity of the non-transformed and first-differenced versions of the chronology suggests that the composite LWB record (1) is a robust and skillful representation of the regional climate, especially for AS $T_{max}$ and (2) maintains the regional temperature signal over the entire instrumental period and is therefore a promising candidate to develop a reconstruction.

### 3.3 Climate reconstruction

We provide a late summer maximum temperature (AS $T_{max}$) reconstruction for the Southern Rocky Mountains that spans the period 1735–2015 (Fig. 3). The predictor time series in the reconstruction model is the AD-sf-detrended composite LWB chronology, which is strongly

and positively calibrated with the predictand data, AS $T_{max}$, during the instrumental period (1907–2015). The LWB chronology explains 42% of the instrumental AS $T_{max}$ variance ($R^2$ = 0.42) from 1907 to 2015 (Fig. 3a, b). Model performance is consistent and time-stable, with both early- and late-period (and vice versa) statistics passing validation tests (Table S6). The strongest model verification occurred by calibrating the model during the late period (1962–2015) and validating over the early period (1907–1961), which is a common finding likely due to the improved accuracy of instrumental data over time (e.g., Maxwell et al. 2017; Harley et al. 2017; Harley and Maxwell 2018).

The AS $T_{max}$ reconstruction for the Southern Rocky Mountains indicates multiple decadal-scale warming and cooling events over the past ca. 120 years (Fig. 3). Comparison of our LWB-based reconstruction with other regional tree-ring-based summer temperature reconstructions indicates overall general commonality of multi-decadal patterns for across many parts of Northern America (Fig. 4). Four of the five warmest single-year anomalies occur from 1924 to 1939, and the 1930s, 1940s, and 1950s all rank as the 2nd, 1st, and 3rd warmest decades, respectively (Fig. 4, Table S7). The warmest decadal anomalies from our reconstruction show agreement with other regional summer temperature reconstructions. The two warmest decadal anomalies (1930s and 1940s) are also within the top five warmest decadal anomalies of reconstructions by Briffa et al. (1992).

The two warmest decadal anomalies (1930s and 1940s) are also within the top five warmest decadal anomalies of reconstructions by Briffa et al. (1992), Trouet et al. (2013), and Wilson et al. (2014, 2019) (Fig. 4). The coldest decadal anomalies from our reconstruction also closely align with those from the LWB-based reconstruction (Wilson et al. 2019), placing the 1760s, 1810s, and 1830s as the three coldest decades. In particular, the MXD-based reconstruction presented by Briffa et al. (1992) shows the most similarity of multi-decadal trends ($r$ = 0.53,

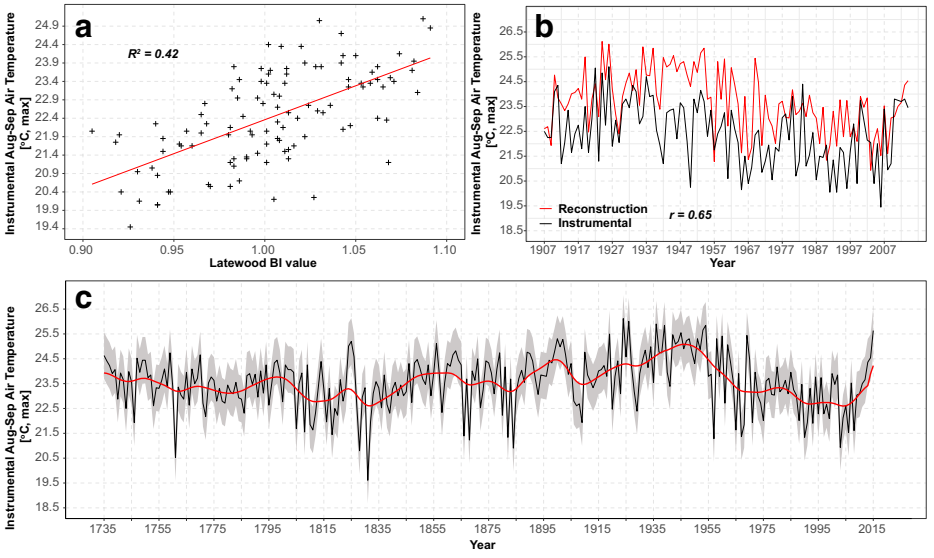


**Fig. 3** Late summer maximum temperature (AS $T_{max}$) reconstruction for the Southern Rocky Mountains, USA. **a** Comparison of regional PRISM 4k AS $T_{max}$ instrumental data (black) and reconstructed AS $T_{max}$ values (red). **b** Scatter plot of the AS $T_{max}$ reconstructed versus instrumental values plotted with linear function (red) and standard error (blue). **c** Reconstruction of August–September $T_{max}$ using the LWB AD-sf composite chronology extending from 1735 to 2015

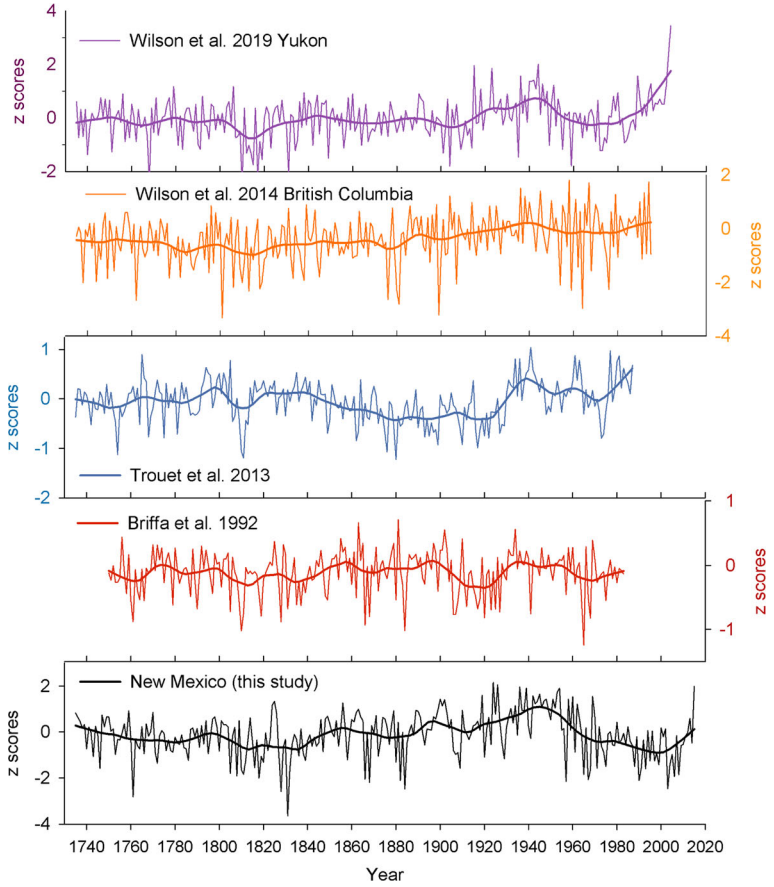


**Fig. 4** Paleotemperature comparisons for western North America. Plotted are the records of the Southern Rocky Mountains LWB AS $T_{max}$ reconstruction presented in this study with Wilson et al.'s (2014) LWB May–August $T_{max}$ record for British Columbia, Canada (orange); Wilson et al.'s (2019) LWB May–August $T_{max}$ record over Yukon Territory, Canada (purple); Trouet et al.'s (2013) ring-width annual $T_{mean}$ record over western North America (blue); and Briffa et al.'s (1992) MXD-based reconstruction of April–September $T_{mean}$ over the American Southwest (red; plotted is grid point #30 from 35° N, 110° W)

$p < 0.01$) over the common reconstructed period. This should be expected due to the regional overlap between our reconstruction and the one presented by Briffa et al. (1992).

Late summer temperature conditions during the twentieth and twenty-first centuries are most notable in the reconstruction from the Southern Rocky Mountains region (Fig. 4). The twentieth century is characterized by steady warming until ca. 1955, with a marked imprint of the Dust Bowl of the 1930s—a series of anomalously dry and warm events experienced throughout portions of the southern plains of the USA into northeast NM (Cook et al. 2014). Our reconstruction, which documents an average decadal anomaly of + 0.88 during this time (Table S7), agrees with the temperature anomalies presented by Cook et al. (2014), who document summer temperature anomalies for the Southern Rocky Mountains (ranging from + 1 to + 2) that are linked to the Dust Bowl of 1934. The period of prolonged warming in the 1930s through the 1950s is consistent with other reconstructions in other areas of North America (Briffa et al. 1992; Trouet et al. 2013; Wiles et al. 2019). This warming is most

comparable with the warming period from 1930 to 1950 presented in the MXD-based reconstruction from Briffa et al. (1992) as well as the reconstruction from Trouet et al. (2013). Primary causes of the Dust Bowl are linked to La Niña conditions in the Pacific Ocean, warm sea surface temperatures (SSTs) in the North Atlantic Ocean, and human-induced land degradation (Seager et al. 2008). A combination of dust storms and the vegetation reduction via the replacement of drought-resistant prairie grass with drought-sensitive wheat during the 1920s are shown to be amplifiers of the anomalously high temperatures (Cook et al. 2009). Most maps detailing the spatial imprint of Dust Bowl temperature anomalies (e.g., Cook et al. 2008) include the easternmost NM counties. Here, we suggest that even at the highest elevations of the Sangre de Cristo Mountains of north-central NM, the Dust Bowl era includes the most pronounced warming event in the context of the past ca. 280 years.

After 1955, a cooling trend occurs for the next ca. 50 years until 2000. The most recent decade is marked by a rapid, extreme warming trend, a rate of change that appears unprecedented since at least 1735. The warming trend of the early twentieth century, followed by a 50-year cooler-than-average period, followed by rapid warming in the last 15 years somewhat differs from many of the more general warming trends documented across the majority of the Southwest US, which suggest continual warming from 1900 until present. Despite this difference, we are confident that the reconstruction we present here is truly representative of the local climate, as seen through the lens of the local instrumental record. At high elevations proximal to cool mountain lakes, such as those sampled in this study, the general warming of the twentieth century is captured but not nearly as pronounced as in other areas of North America. While our reconstruction is in close agreement with Wilson et al.'s (2019) reconstruction from the Yukon Territory, Canada, the Southern Rocky Mountains reconstruction does not show a dramatic warming trend in the beginning of the twenty-first century, except for the last ca. 5 years of the record. Comparison of this period trend in both reconstructions begins to address the varying magnitudes of warming at different latitudes within North America, but further comparisons are ultimately limited by the non-contemporary lengths of the records (the Yukon reconstruction ending in 2004). Overall multi-decadal trends between our reconstruction and the reconstruction presented by Wilson et al. (2014) for southern British Columbia are relatively similar, but they do display some misalignment of cold decades. The dissimilarities between maximum summer temperatures between southern British Columbia and the Southern Rocky Mountains suggest implications of broader climate dynamics across North America that warrants future examination.

The reconstruction also shows indications of cool periods aligning with the last ca. 100 years of the Little Ice Age (LIA; ca. 1300–1850 CE), a period of below-average temperatures. The LIA has been the focus of many studies, and recent work suggests that the onset, duration, and intensity of the LIA appear to have subregional spatial difference (e.g., Wahl and Smerdon 2012; Neukom et al. 2019). Because our reconstruction only covers the last ca. 100 years of the LIA, relative comparisons with other reconstructions documenting the full duration of this period are precluded by the length of our record. Nonetheless, we demonstrate contrasting cool and warm phases within the latter part of the LIA. The trend of the reconstruction shows a cooling period from 1735 to 1835, then slightly warmer-than-average conditions from 1840 to 1885. After 1885, increasingly warming conditions persist until 1955.

In the Southern Rocky Mountains region, we discovered close coupling between maximum summer temperature and hydroclimate over the past ca. 280 years. We note substantial association between our AS $T_{max}$ reconstruction and the summer drought reconstruction from

El Malpais, NM (34.79° N, 108.00° W; Oliver et al. 2019) with regard to intensity of anomalies, especially since the turn of the twentieth century (Fig. 5). We attribute this strong coupling between temperature and hydroclimate to the growing influence of modern (the start of the instrumental record to present) increasing surface air temperatures on the hydrologic cycle, as this is recently documented across the American Southwest (Weiss et al. 2009; Cayan et al. 2010; Udall and Overpeck 2017). The decreased synchrony between either wet + cool or dry + warm events in the earlier parts of the record suggests that the relationship between temperature and hydroclimate in this region was more decoupled prior to the Industrial Revolution, and hence, this phenomenon is specific to the twentieth-twenty-first centuries (at least within the context of the past 280 years). The shift in synchrony between our temperature reconstruction and Oliver et al.'s (2019) hydroclimate reconstruction after ca. 1835 alludes to the influence of anthropogenic warming on the modern hydrologic system in this region. Based on this trend, we suggest that more well-validated, long-term temperature proxy records are increasingly important in areas such as the Southwest US for placing modern hot droughts into historical context, as has been shown for the Midwest US (Maxwell and Harley 2017). The multi-millennial hydroclimate reconstruction by Oliver et al. (2019) extends from 2015 back to 492 BCE. Although our record currently extends to the 1730s, developing a longer-term record could be possible across the region, especially at high-elevation sites in the Sangre de Cristo Mountains. In particular, we discovered an abundance of submerged, remnant Engelmann spruce logs at the SLE site (Figure S5). Future efforts should be placed on extending the Southern Rocky Mountains temperature reconstruction back in time by incorporating remnant and subfossil spruce material. Such an effort would allow for longer-term understandings of hydroclimate-drought relationships, especially comparing the current warming trend with conditions during the Medieval climatic anomaly and LIA.

Within the context of developing temperature reconstruction networks over greater spatial extents, LWB offers an efficient and effective alternative tree-ring parameter to MXD for developing temperature-sensitive chronologies that account for periods of time that should be interpreted cautiously due to low sample depth. These periods include prior to 1400 CE and post 1988 CE (Anchukaitis et al. 2017). While this reconstruction is limited from 1735 to 2015, we do account for the most recent decades. Although the reconstruction we present here offers valuable insight regarding temperature variability over the Southern Rocky Mountains during the last 280 years, this study would be improved by additional sampling efforts resulting in the ability to evaluate longer-term, multi-centennial variability in the region. While we demonstrate the successful application of BI methods on living Engelmann spruce located at the southern range limit for the species, further investigation regarding the efficacy of BI on remnant samples (e.g., Wilson et al. 2017b) must be examined. The three sites from this study are all located up-slope from Alpine lakes, which contain many large, likely old, logs as a result from prolonged geomorphological events (e.g., rock slide, avalanche) (Figure S5). Future sampling of these logs will allow for the development of a composite chronology that extends further back in time with increased sample depth. However, one of the major issues using BI methods on non-living trees is the increased presence of discoloration due to decay and algal/fungal staining (Björklund et al. 2014; Wilson et al. 2017b). While this issue may be remedied by pre-treating discolored cores with a combination of acetone and ethanol (Rydval et al. 2014), living tree samples are often generally brighter than samples from older remnant material (Björklund et al. 2014). To reduce potential bias resultant from brightness differences between samples of live and dead trees, the ΔBI metric may be of increased importance here. As LWB and ΔBI exhibit similar relationships to monthly $T_{max}$, the ΔBI metric may have

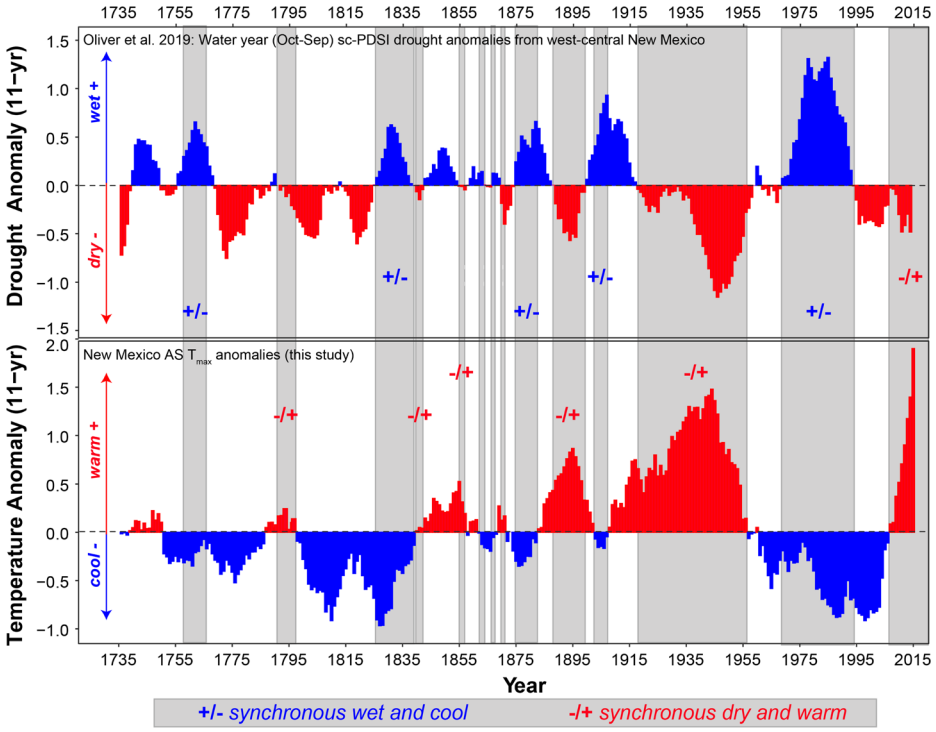


**Fig. 5** Hydroclimate-temperature comparisons for the Southern Rocky Mountains. Comparison of 11-year anomalies of (top) west-central New Mexico hydroclimate conditions presented by Oliver et al. (2019) and (bottom) reconstructed AS $T_{max}$ presented in this study over the period of overlap (1735–2015). Identified is a period of coupled wet + cool and dry + warm conditions across the region

additional use for investigating BI methods on subfossil wood and combining remnant BI chronologies with BI chronologies from live trees.

To our knowledge, this study is the first instance of a temperature reconstruction using BI methods at the mid-latitudes of North America. While attempts have been made to develop chronology networks in the Western US (Schweingruber 1988), these tree line networks do not include BI-derived data. Although a considerable number of BI-derived Engelmann spruce chronologies exist in Western Canada (e.g., Wilson et al. 2014), future efforts should also be placed towards extending the BI data network towards the southern half of the natural species range (e.g., Utah, Colorado, Wyoming, Idaho, Montana, USA). Such an effort would enable connections between the record presented here for the Southern Rocky Mountains, and the BI-derived temperature records from the Yukon (Wilson et al. 2019) and British Columbia (Wilson and Luckman 2003), thus resulting in the ability to consider a number of BI-derived Engelmann spruce chronologies, exist in Western Canada (e.g., Wilson et al. 2014); future efforts should also be placed towards extending the BI data network towards the southern half of the natural species range (e.g., Utah, Colorado, Wyoming, Idaho, Montana, USA). Such an effort would enable connections between the record presented here for the Southern Rocky Mountains, and the BI-derived temperature records from the Yukon (Wilson et al. 2019) and British Columbia (Wilson and Luckman 2003), thus resulting in the ability to produce broad-scale, long-term temperature information for western North America during this period of rapidly changing climate.

## 4 Conclusions

In this study, we demonstrate the successful application of BI methods on tree cores collected across three high-elevation, mid-latitude populations of Engelmann spruce located at the species southern geographical range limit. To our knowledge, this is the first published study to explore the application of this technique in the mid-latitudes of North America for the purpose of developing a temperature reconstruction. We reconstructed late summer temperatures spanning from 1735 until 2015 using the LWB metric, and we demonstrate that BI metrics can provide robust climate proxy data in the mid-latitudes of the USA. As this study shows both spatially and temporally resolved temperature responses for the southern Rocky Mountains region of the USA, this study does suggest that BI methods are useful for producing temperature-responsive parameters which are alternative to MXD. In possessing many attractive qualities such as cost and time efficiency, which do not appear to have exhibited a divergence issue as seen in other tree-ring metrics, BI methods offer an important alternative approach to spatially improving under-represented locations within pre-existing temperature networks that rely heavily on MXD. In places such as the American Southwest, where even MXD records are spatially and temporally limited, further wide-scale examination of BI methods is necessary for more adequately capturing broader regional climate trends and placing current warming trends into greater spatial and historical contexts.

**Acknowledgments** JT Maxwell and students were supported during the field sample collection by the Indiana University Institute for Advanced Study. We would like thank Lamar Gillespie, George Harley, Lola Harley, Douglas Heruska, Randy Matheaus, Joshua Oliver, Karly Schmidt, Kerri Spuller, Brandon Strange, and Michael Thornton for their assistance with the data collection, Rob Wilson, and the two anonymous reviewers for their very thorough edits and suggestions that improved earlier drafts of this manuscript.

**Funding information** We would like to thank the University of Idaho and Indiana University for the financial support of this project.

## References

Akaike H (1974) A new look at the statistical model identification. IEEE Trans Autom Control 19(6):716–723

Alexander R, Sheppard W (1984) Silvicultural characteristics of Engelmann spruce. USDA Forest Service general technical report RM 114

Anchukaitis KJ, D'Arrigo RD, Andreu-Hayles L, Frank D, Verstege A, Curtis A, Buckley BM, Jacoby GC, Cook ER (2013) Tree-ring-reconstructed summer temperatures from northwestern North America during the last nine centuries. J Clim 26(10):3001–3012

Anchukaitis KJ, Wilson R, Briffa KR, Büntgen U, Cook ER, D'Arrigo R, Davi N, Esper J, Frank D, Gunnarson BE et al (2017) Last millennium Northern Hemisphere summer temperatures from tree rings: part ii, spatially resolved reconstructions. Quat Sci Rev 163:1–22

Biondi F, Perkins D, Cayan D, Hughes M (1999) July temperature during the second millennium reconstructed from Idaho tree rings. Geophys Res Lett 26(10):1445–1448

Björklund J, Gunnarson BE, Seftigen K, Esper J, Linderholm H (2014) Blue intensity and density from northern fennoscandian tree rings, exploring the potential to improve summer temperature reconstructions with earlywood information. Clim Past 10(2):877–885

Björklund J, Gunnarson BE, Seftigen K, Zhang P, Linderholm HW (2015) Using adjusted blue intensity data to attain high-quality summer temperature information: a case study from central scandinavia. The Holocene 25(3):547–556

Björklund J, Seftigen K, Schweingruber F, Fonti P, von Arx G, Bryukhanova MV, Cuny HE, Carrer M, Castagneri D, Frank DC (2017) Cell size and wall dimensions drive distinct variability of earlywood and latewood density in Northern Hemisphere conifers. New Phytol 216(3):728–740

Björklund J, von Arx G, Nievergelt D, Wilson R, Van den Bulcke J, Günther B, Loader N, Rydval M, Fonti P, Scharnweber T, et al. (2019) Scientific merits and analytical challenges of tree-ring densitometry. Rev Geophys
Blunden J, Arndt DS (2016) State of the climate in 2016. Bull Am Meteorol Soc 98(8):Si–S280
Briffa KR, Jones PD, Schweingruber FH (1988) Summer temperature patterns over Europe: a reconstruction from 1750 A.D. based on maximum latewood density indices of conifers. Quat Res 30(1):36–52
Briffa KR, Jones P, Schweingruber F (1992) Tree-ring density reconstructions of summer temperature patterns across western North America since 1600. J Clim 5(7):735–754
Briffa KR, Osborn TJ, Schweingruber FH, Harris IC, Jones PD, Shiyatov SG, Vaganov EA (2001) Low-frequency temperature variations from a northern tree ring density network. J Geophys Res Atmos 106(D3):2929–2941
Briffa KR, Osborn TJ, Schweingruber FH, Jones PD, Shiyatov SG, Vaganov EA (2002) Tree-ring width and density data around the Northern Hemisphere: part 1, local and regional climate signals. The Holocene 12(6):737–757
Brookhouse M, Graham R (2016) Application of the minimum blue-intensity technique to a Southern-Hemisphere conifer. Tree-Ring Res 72(2):103–107
Buckley BM, Hansen KG, Griffin KL, Schmiege S, Oelkers R, D'Arrigo RD, Stahle DK, Davi N, Nguyen TQT, Le CN et al (2018) Blue intensity from a tropical conifers annual rings for climate reconstruction: an ecophysiological perspective. Dendrochronologia 50:10–22
Büntgen U, Frank D, Wilson R, Carrer M, Urbinati C, Esper J (2008) Testing for tree-ring divergence in the European Alps. Glob Chang Biol 14(10):2443–2453
Campbell R, McCarroll D, Loader NJ, Grudd H, Robertson I, Jalkanen R (2007) Blue intensity in Pinus sylvestris tree-rings: developing a new palaeoclimate proxy. The Holocene 17(6):821–828
Cayan DR, Kammerdiener SA, Dettinger MD, Caprio JM, Peterson DH (2001) Changes in the onset of spring in the Western United States. Bull Am Meteorol Soc 82(3):399–416
Cayan DR, Das T, Pierce DW, Barnett TP, Tyree M, Gershunov A (2010) Future dryness in the southwest us and the hydrology of the early 21st century drought. Proc Natl Acad Sci 107(50):21271–21276
Cook ER, Kairiukstis LA (2013) Methods of dendrochronology: applications in the environmental sciences. Springer Science & Business Media
Cook ER, Meko DM, Stahle DW, Cleaveland MK (1999) Drought reconstructions for the continental United States. J Clim 12(4):1145–1162
Cook BI, Miller RL, Seager R (2008) Dust and sea surface temperature forcing of the 1930s Dust Bowl drought. Geophys Res Lett 35(8)
Cook BI, Miller RL, Seager R (2009) Amplification of the North American Dust Bowl drought through human-induced land degradation. Proc Natl Acad Sci 106(13):4997–5001
Cook ER, Palmer JG, Ahmed M, Woodhouse CA, Fenwick P, Zafar MU, Wahab M, Khan N (2013) Five centuries of upper indus river flow from tree rings. J Hydrol 486:365–375
Cook BI, Smerdon JE, Seager R, Cook ER (2014) Pan-continental droughts in North America over the last millennium. J Clim 27(1):383–397
D'Arrigo R, Wilson R, Liepert B, Cherubini P (2008) On the divergence problem in northern forests: a review of the tree-ring evidence and possible causes. Glob Planet Chang 60(3–4):289–305
Daly C, Neilson RP, Phillips DL (1994) A statistical-topographic model for mapping climatological precipitation over mountainous terrain. J Appl Meteorol 33(2):140–158
Data UC (2019) Temperature - precipitation - sunshine - snowfalls
Davi NK, Jacoby GC, Wiles GC (2003) Boreal temperature variability inferred from maximum latewood density and tree-ring width data, Wrangell Mountain region, Alaska. Quat Res 60(3):252–262
Durbin J, Watson GS (1971) Testing for serial correlation in least squares regression. iii. Biometrika 58(1):1–19
Fritts H (1976) Tree rings and climate. Elsevier
Fuentes M, Salo R, Björklund J, Seftigen K, Zhang P, Gunnarson B, Aravena JC, Linderholm HW (2018) A 970-year-long summer temperature reconstruction from Rogen, west-central Sweden, based on blue intensity from tree rings. The Holocene 28(2):254–266
Garfin G, Franco G, Blanco H, Comrie A, Gonzalez P, Piechota T, Smyth R,Waskom R (2014) Southwest: the third National Climate Assessment. In: Climate change impacts in the United States: the third National Climate Assessment, US Global Change Research Program, pp 462–486
Gindl W, Grabner M, Wimmer R (2000) The influence of temperature on latewood lignin content in treeline Norway spruce compared with maximum density and ring width. Trees 14(7):409–414
Guttman L (1954) Some necessary conditions for common-factor analysis. Psychometrika 19(2):149–161
Harley GL, Maxwell JT (2018) Current declines of Pecos river (New Mexico, USA) streamflow in a 700-year context. The Holocene 28(5):767–777
Harley GL, Maxwell JT, Larson E, Grissino-Mayer HD, Henderson J, Huffman J (2017) Suwannee river flow variability 1550–2005 CE reconstructed from a multispecies tree-ring network. J Hydrol 544:438–451

Harley GL, Maxwell RS, Black BA, Bekker MF (2020) A multi-century, tree-ring-derived perspective of the north cascades (USA) 2014–2016 snow drought. Climatic Change pp 1–17
Heeter KJ, Harley GL, Van De Gevel SL, White PB (2019) Blue intensity as a temperature proxy in the Eastern United States: a pilot study from a southern disjunct population of Picea rubens (Sarg.). Dendrochronologia 55:105–109
Holmes RL (1983) Computer-assisted quality control in tree-ring dating and measurement
Jacoby GC, D'Arrigo R (1989) Reconstructed Northern Hemisphere annual temperature since 1671 based on high-latitude tree-ring data from North America. Clim Chang 14(1):39–59
Jardine A, Merideth R, Black M, LeRoy S (2013) Assessment of climate change in the Southwest United States: a report prepared for the National Climate Assessment. Island
Jones PD, New M, Parker DE, Martin S, Rigor IG (1999) Surface air temperature and its changes over the past 150 years. Rev Geophys 37(2):173–199
Kaczka RJ, Spyt B, Janecka K, Beil I, Büntgen U, Scharnweber T, Nievergelt D, Wilmking M (2018) Different maximum latewood density and blue intensity measurements techniques reveal similar results. Dendrochronologia 49:94–101
Kaiser HF (1960) The application of electronic computers to factor analysis. Educ Psychol Meas 20(1):141–151
Larsson L (2014) CooRecorder and CDendro programs of the CooRecorder/CDendro package version 7.7
Linderholm HW, Björklund J, Seftigen K, Gunnarson BE, Fuentes M (2015) Fennoscandia revisited: a spatially improved tree-ring reconstruction of summer temperatures for the last 900 years. Clim Dyn 45(3–4):933–947
Little EL, Viereck LA (1971) Atlas of United States trees, vol 5. US Dept. of Agriculture, Forest Service
Luckman B, Wilson R (2005) Summer temperatures in the Canadian rockies during the last millennium: a revised record. Clim Dyn 24(2–3):131–144
Maxwell JT, Harley GL (2017) Increased tree-ring network density reveals more precise estimations of sub-regional hydroclimate variability and climate dynamics in the Midwest, USA. Clim Dyn 49(4):1479–1493
Maxwell RS, Harley GL, Maxwell JT, Rayback SA, Pederson N, Cook ER, Bar-clay DJ, Li W, Rayburn JA (2017) An interbasin comparison of tree-ring reconstructed streamflow in the Eastern United States. Hydrol Process 31(13):2381–2394
McCarroll D, Pettigrew E, Luckman A, Guibal F, Edouard JL (2002) Blue reflectance provides a surrogate for latewood density of high-latitude pine tree rings. Arct Antarct Alp Res 34(4):450–453
Melvin TM, Briffa KR (2008) A signal-free approach to dendroclimatic standardisation. Dendrochronologia 26(2):71–86
Melvin TM, Briffa KR, Nicolussi K, Grabner M (2007) Time-varying-response smoothing. Dendrochronologia 25(1):65–69
Mooney H, Larigauderie A, Cesario M, Elmquist T, Hoegh-Guldberg O, Lavorel S, Mace GM, Palmer M, Scholes R, Yahara T (2009) Biodiversity, climate change, and ecosystem services. Curr Opin Environ Sustain 1(1):46–54
Neukom R, Steiger N, Gómez-Navarro JJ, Wang J, Werner JP (2019) No evidence for globally coherent warm and cold periods over the preindustrial Common Era. Nature 571(7766):550–554
NOAA (2016) National Centers for Environmental information. Climate at a Glance: Regional Mapping. https://www.ncdc.noaa.gov, https://www.ncdc.noaa.gov/cag/
Oliver JS, Harley GL, Maxwell JT (2019) 2,500 years of hydroclimate variability in New Mexico, USA. Geophys Res Lett 46(8):4432–4440
Parker M, Henoch W (1971) The use of Engelmann spruce latewood density for dendrochronological purposes. Can J For Res 1(2):90–98
Rydval M, Larsson LÅ, McGlynn L, Gunnarson BE, Loader NJ, Young GH, Wilson R (2014) Blue intensity for dendroclimatology: should we have the blues? Experiments from Scotland. Dendrochronologia 32(3):191–204
Salzer MW, Kipfmueller KF (2005) Reconstructed temperature and precipitation on a millennial timescale from tree-rings in the southern Colorado Plateau, USA. Clim Chang 70(3):465–487
Schneider L, Smerdon JE, Büntgen U, Wilson RJ, Myglan VS, Kirdyanov AV, Esper J (2015) Revising midlatitude summer temperatures back to A.D. 600 based on a wood density network. Geophys Res Lett 42(11):4556–4562
Schweingruber F (1988) A new dendroclimatic network for western North America. Dendrochronologia 6:171–180
Schweingruber FH, Briffa KR (1996) Tree-ring density networks for climate reconstruction. In: Climatic variations and forcing mechanisms of the last 2000 years, Springer, pp 43–66
Schweingruber F, Briffa K, Nogler P (1993) A tree-ring densitometric transect from Alaska to Labrador. Int J Biometeorol 37(3):151–169
Seager R, Kushnir Y, Ting M, Cane M, Naik N, Miller J (2008) Would advance knowledge of 1930s SSTs have allowed prediction of the Dust Bowl drought? J Clim 21(13):3261–3281

Sheppard PR, Graumlich LJ, Conkey LE (1996) Reflected-light image analysis of conifer tree rings for reconstructing climate. The Holocene 6(1):62–68
Speer JH (2010) Fundamentals of tree-ring research. University of Arizona Press
Stoffel M, Khodri M, Corona C, Guillet S, Poulain V, Bekki S, Guiot J, Luckman BH, Oppenheimer C, Lebas N et al (2015) Estimates of volcanic-induced cooling in the Northern Hemisphere over the past 1,500 years. Nat Geosci 8(10):784
Stokes M, Smiley T (1968) An introduction to tree-ring dating. University of Chicago Press, Chicago
Thornton PK, Ericksen PJ, Herrero M, Challinor AJ (2014) Climate variability and vulnerability to climate change: a review. Glob Chang Biol 20(11):3313–3328
Trouet V, Van Oldenborgh GJ (2013) KNMI Climate Explorer: a Web-based research tool for high-resolution paleoclimatology. Tree-Ring Res 69(1):3–14
Trouet V, Diaz H, Wahl E, Viau A, Graham R, Graham N, Cook E (2013) A 1500-year reconstruction of annual mean temperature for temperate North America on decadal-to-multidecadal time scales. Environ Res Lett 8(2):024008
Udall B, Overpeck J (2017) The twenty-first century Colorado River hot drought and implications for the future. Water Resour Res 53(3):2404–2418
Vinod HD, Lopez-de Lacalle J (2009) Maximum entropy bootstrap for time series: the meboot R package. J Stat Softw 29(5):1–19
Wahl ER, Smerdon JE (2012) Comparative performance of paleoclimate field and index reconstructions derived from climate proxies and noise-only predictors. Geophys Res Lett 39(6)
Weiss JL, Castro CL, Overpeck JT (2009) Distinguishing pronounced droughts in the southwestern United States: seasonality and effects of warmer temperatures. J Clim 22(22):5918–5932
Westerling AL, Hidalgo HG, Cayan DR, Swetnam TW (2006) Warming and earlier spring increase western us forest wildfire activity. Science 313(5789):940–943
Wigley TM, Briffa KR, Jones PD (1984) On the average value of correlated time series, with applications in dendroclimatology and hydrometeorology. J Clim Appl Meteorol 23(2):201–213
Wiles GC, D'Arrigo RD, Barclay D, Wilson RS, Jarvis SK, Vargo L, Frank D (2014) Surface air temperature variability reconstructed with tree rings for the Gulf of Alaska over the past 1200 years. The Holocene 24(2): 198–208
Wiles G, Charlton J, Wilson RJ, D'Arrigo R, Buma B, Krapek J, Gaglioti BV, Wiesenberg N, Oelkers R (2019) Yellow-cedar blue intensity tree ring chronologies as records of climate, Juneau, Alaska, USA. Can J For Res
Wilson RJ, Luckman BH (2003) Dendroclimatic reconstruction of maximum summer temperatures from upper treeline sites in interior British Columbia, Canada. The Holocene 13(6):851–861
Wilson R, D'Arrigo R, Buckley B, Büntgen U, Esper J, Frank D, Luckman B, Payette S, Vose R, Youngblut D (2007a) A matter of divergence: tracking recent warming at hemispheric scales using tree ring data. J Geophys Res Atmos 112(D17)
Wilson R, Wiles G, D'Arrigo R, Zweck C (2007b) Cycles and shifts: 1,300 years of multi-decadal temperature variability in the Gulf of Alaska. Clim Dyn 28(4):425–440
Wilson R, Rao R, Rydval M, Wood C, Larsson LÅ, Luckman BH (2014) Blue intensity for dendroclimatology: the BC blues: a case study from British Columbia, Canada. The Holocene 24(11):1428–1438
Wilson R, Anchukaitis K, Briffa KR, Büntgen U, Cook E, D'Arrigo R, Davi N, Esper J, Frank D, Gunnarson B et al (2016) Last millennium Northern Hemisphere summer temperatures from tree rings: part i: the long term context. Quat Sci Rev 134:1–18
Wilson R, D'Arrigo R, Andreu-Hayles L, Oelkers R, Wiles G, Anchukaitis K, Davi N (2017a) Experiments based on blue intensity for reconstructing North Pacific temperatures along the Gulf of Alaska. Clim Past
Wilson R, Wilson D, Rydval M, Crone A, Büntgen U, Clark S, Ehmer J, Forbes E, Fuentes M, Gunnarson BE et al (2017b) Facilitating tree-ring dating of historic conifer timbers using blue intensity. J Archaeol Sci 78: 99–111
Wilson R, Anchukaitis K, Andreu-Hayles L, Cook E, D'Arrigo R, Davi N, Haberbauer L, Krusic P, Luckman B, Morimoto D, et al. (2019) Improved dendroclimatic calibration using blue intensity in the southern Yukon. The Holocene p 0959683619862037
Zang C, Biondi F (2015) treeclim: an R package for the numerical calibration of proxy-climate relationships. Ecography 38(4):431–436

## Affiliations

**Karen J. Heeter[1] · Grant L. Harley[1] · Justin T. Maxwell[2,3] · James H. McGee[1] · Trevis J. Matheus[4]**

✉ Karen J. Heeter
kheeter@uidaho.edu

[1] Idaho Tree-Ring Laboratory, Department of Geography, University of Idaho, Moscow, ID 83843, USA

[2] Environmental Tree-Ring Laboratory, Department of Geography, Indiana University, Bloomington, IN 4740, USA

[3] Harvard Forest, Harvard University, Petersham, MA 01336, USA

[4] Cal-Dendro Tree-Ring Laboratory, Department of Geography and Environment, California State University, Fullerton, Fullerton, CA 92831, USA